NJC

PAPER

View Article Online
View Journal | View Issue

Cite this: *New J. Chem.*, 2019, **43**, 6063

Air/water interfacial growth of Pt nanothorns anchored *in situ* on macroscopic freestanding CNT thin film for efficient methanol oxidation†

Wei Zhang,[ab] Lei Zhang,*[b] Gui Zhang,[b] Peng Xiao,[b] Youju Huang,[b] Min Qiang*[a] and Tao Chen*[b]

Received 24th January 2019,
Accepted 14th March 2019

DOI: 10.1039/c9nj00437h

rsc.li/njc

As one widely used anode electrocatalyst for alcohol oxidation, Pt nanoparticles have been paid a lot of attention with the aim of improving their catalytic properties by tuning their sizes, morphologies, and components. One-dimensional (1D) Pt nanostructures possess sufficient active crystal lattices and interfacial electron transfer pathways, and usually show excellent catalytic properties. At present, there are still large challenges relating to the controllable synthesis of 1D Pt nanostructures and their effective loading on appropriate supports, which limit the practical catalytic performances of Pt nanoparticles. Herein, one-dimensional Pt nanothorns (NTs) of about 5.9 nm diameter are synthesized *via* a unique air/water interfacial process and are anchored densely *in situ* on the surface of supporting carbon nanotubes (CNTs). The resultant macroscopic freestanding CNTs/PtNTs hybrid film with sufficient active sites and a large electrochemical active surface area of 190.5 cm^2 mg^{-1} exhibits efficient electrocatalytic ability for methanol oxidation. This interfacial fabrication strategy provides a simple and effective means to prepare a PtNT composite with high catalytic activity and stability, showing good potential for application in flexible alcohol fuel cells.

1. Introduction

Recently, direct-methanol fuel cells (DMFCs) have attracted considerable attention because of their high energy density and cleanliness, coupled with the convenient storage and carriage of methanol.[1] The electrocatalyst is one of the key points influencing the performance of a DMFC. Highly catalytic activity and good durability are two significant factors for evaluating an electrocatalyst. In past decades, various catalysts with high catalytic ability for alcohol oxidation have been reported to improve the energy density and power of fuel cells: for example, noble metal catalysts.[2–5] Meanwhile, platinum nanoparticle (Pt NP) catalysts have been widely used as anode electrocatalysts for DMFC. To efficiently utilize the expensive Pt catalyst, highly active Pt NPs with different sizes or morphologies are synthesized and loaded on appropriate supporting materials.[6,7] Tiny Pt nanoparticles attached on carbon nanotubes showed high catalytic ability for methanol oxidation.[8] Some Pt nanoparticles with a special morphology usually have active crystal planes. For example, one-dimensional Pt nanowires usually have rich active catalytic sites sufficiently exposed to the electrolyte in the interface as well as facile pathways for electron transfer.[9,10] Much work has been reported on the preparation of Pt nanowires,[11] such as the solvothermal method,[12] template method[13] and wet chemistry method.[14] Conventional synthesis processes to produce Pt nanowires are usually sophisticated and it is sometimes difficult to reproduce results. In addition, the dispersiveness of Pt nanoparticles is also significant for the catalytic performance. It is necessary to load nanoparticles onto an appropriate support with a high specific surface area, such as carbon nanomaterials[15–19] or conductive polymers.[20,21]

Unlike the reaction process in bulk solution,[22] the interfacial reaction occurs only on the boundary between two phases, providing the possibility of producing some unique nanostructures. For example, an asymmetrical Ag@Ag/S hybrid film was prepared stably on an air/water interface.[23] In our previous work, the air/water interfacial reaction was employed to synthesize effectively tiny Au nanoparticles that were *in situ* loaded densely on CNT film.[24] An interfacial reaction occurring in a confined space usually shows a slow reaction rate due to the diffusion of reactive agents toward the interface. It will likely be possible to promote the specific growth of some lattices at the interface under the assistance of capping agents.

[a] *College of Chemistry and Chemical Engineering, Wuhan University of Science and Technology, 947 Peace Avenue, Wuhan 430081, China. E-mail: minqiang@aliyun.com*

[b] *Key Laboratory of Bio-based Polymeric Materials Technology and Application of Zhejiang Province, Ningbo Institute of Materials Technology and Engineering, Chinese Academy of Sciences, Ningbo 315201, P. R. China. E-mail: zhanglei@nimte.ac.cn, taochen@nimte.ac.cn*

† Electronic supplementary information (ESI) available. See DOI: 10.1039/c9nj00437h

Herein, an air/water interfacial reaction strategy is presented to conveniently synthesize Pt nanothorns. A macroscopic freestanding CNT film floating on the surface of a solution is used as a 2D interfacial support for the *in situ* growth and attachment of Pt nanothorns (PtNTs). PtNTs attach densely on the freestanding CNT film, achieving a robust CNTs/PtNTs hybrid by a one-step method. The resultant CNTs/PtNTs hybrid has a high specific surface area and active crystal planes, showing efficient catalysis for alcohol oxidation. This CNTs/PtNTs hybrid also exhibits flexible features and a convenient transfer operation, with good potential for applications in flexible alcohol fuel cells[25,26] and wearable soft power devices.[27–29]

2. Experimental

2.1 Materials

All reagents were used as received without further purification. Hexachloroplatinic acid hexahydrate ($H_2PtCl_6{\cdot}6H_2O$, 99.95%), poly(vinyl pyrrolidone) (PVP, M.W. = 60 000), commercial platinum/carbon (Pt/C, 5%) and formic acid (HCOOH, 98%) were purchased from J&K Scientific Ltd (Shanghai). Sodium hydroxide (98%), ethanol (AR), and sulfuric acid (98%) were provided by Sinopharm Chemical Reagent Co., Ltd (Shanghai). Multi-walled carbon nanotubes (CNTs, diameter: 10–30 nm; length: 10–30 μm; COOH: 2 wt%) were supplied by Chengdu Organic Chemistry Co., Ltd. All aqueous solutions are prepared using distilled water.

2.2 Preparation of CNT thin film on the air/water interface

The freestanding CNT film is prepared according to the previous work with some modifications.[30] Briefly, 5 mg of CNTs is dispersed homogenously in 25 mL of ethanol solution by 30 min of ultrasonication. The resultant mixed dispersion is ejected slowly onto the water surface by means of a syringe. Subsequently, a loose freestanding CNT film floats stably on the surface of the water. The resultant CNT film is pressed compactly under the capillary force driven by a sucking sponge. Finally, a compacted CNT thin film is prepared and can be transferred stably to another solution surface.

2.3 Preparation of CNTs/PtNTs thin film

Typically, 0.2 mL of 0.1 M H_2PtCl_6 aqueous solution is added into 13.4 mL of PVP aqueous solution (1.1 mg mL^{-1}) and a uniform yellow solution is obtained. 0.4 mL of formic acid is dissolved into the above solution and forms the growth solution for the PtNTs. The prepared freestanding CNT film is transferred onto the surface of the above growth solution. After the reaction has finished, a macroscopic freestanding CNTs/PtNTs hybrid film is obtained. The hybrid film is transferred onto a silicon wafer and blow-dried with nitrogen. Then the film is cleaned by immersing it alternately into ethanol and distilled water three times. After drying at 45 °C for 2 h, the hybrid film can be used for further characterization or other experiments.

2.4 Characterization

Observations on the microstructure of CNTs/PtNTs film were conducted by SEM (S4800 scanning electron microscope) and TEM (JEOL JEM 2010, Japan). The crystalline structure of Pt nanothorns was characterized by X-ray diffraction (XRD) with Cu-Kα radiation, using an automated X-ray diffractometer (Bruker AXS D8, Germany). The elemental compositions of the composite film were analysed by X-ray photoelectron spectroscopy (AXIS ULTRA DLD, Kratos Analytical Ltd, Manchester, UK). The weight of PtNTs in the composite film was determined by inductively coupled plasma mass spectrometry (ICP-MS) (NexION 300X, USA).

The electrochemical properties of the CNTs/PtNTs film were studied by a CHI 660D electrochemical workstation (CH Instruments, Chenhua Co, Shanghai, China) with a conventional three-electrode system. The glassy carbon electrode was polished successively with 1.0 μm, 0.05 μm α-alumina powder before sonication washing with distilled water. The CNTs/PtNTs composite film was transferred stably onto the surface of a glassy carbon electrode and used as the working electrode after blow-drying with nitrogen gas. An Ag/AgCl electrode and a Pt electrode were employed as reference electrode and counter electrode, respectively. All the electrolytic solutions were purged with nitrogen for at least 10 min to obtain an N_2-protected solution. For comparison, commercial Pt/C was dispersed in distilled water and dropped onto the surface of a glassy carbon electrode. After drying completely, 5 μL of Nafion aqueous solution (5 wt%) was dropped onto the electrode surface of the Pt/C coated electrode and dried at room temperature before further measurement.

3. Results and discussion

The air/water interfacial reaction strategy for fabricating CNTs/PtNTs hybrid is illustrated in Scheme 1. A freestanding CNT assembled film is transferred stably onto the surface of the H_2PtCl_6 solution and used as a 2D interfacial support for the growth of PtNTs (Scheme 1A and B). $PtCl_6^{2-}$ ions diffuse into CNTs film and fill the porous CNTs network. Owing to the reduction by formic acid of $PtCl_6^{2-}$ ions, Pt atoms are produced continuously and are simultaneously absorbed on the surface of the CNTs. The Pt atoms attached on the CNTs serve as nucleation centers for the gradual growth of PtNTs (Scheme 1C). The resultant

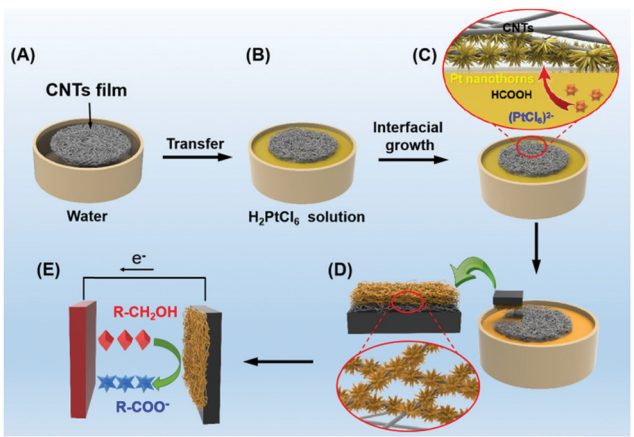

Scheme 1 A schematic illustration of the interfacial fabrication of the CNTs/PtNTs composite film for electrocatalytic alcohol oxidation.

PtNTs densely attach on the surface of the CNTs, leading to the formation of a freestanding CNTs/PtNTs hybrid film (Scheme 1D). Due to its good mechanical stability and flexibility, the prepared CNTs/PtNTs film can be transferred stably and used directly as a catalyst membrane for alcohol oxidation (Scheme 1E).[31] The achieved macroscopic CNTs/PtNTs hybrid film has a large area of up to dozens of square centimeters (Fig. 1A, inset). The morphology of the CNTs/PtNTs hybrid film was characterized by SEM and TEM upon transfer onto the silicon wafer. It can clearly be observed that the CNTs are coated with a layer of rugged nanoshell, leading to the rough surface and large diameter of the CNTs (Fig. 1A). The high-resolution SEM image shows that the nanoshell consists of nanothorn structures (Fig. 1B). As shown in the SEM image, the average diameter of a Pt nanothorn is about 5.9 nm, which is smaller than the size of a CNT (20–30 nm diameter). In addition, the TEM images in Fig. 1C and Fig. S1 (ESI†) also display that the surface of the CNTs is wrapped completely by the dense nanothorn shell, implying a high specific surface area. Furthermore, the distinct lattice planes of the nanothorn shell in the high-resolution TEM image indicate ordered crystal structures (the inset in Fig. 1C). The composition of the CNTs/PtNTs film was further characterized by XPS spectra. In the XPS spectrum, there are strong peaks around 73 eV attributed to Pt 4f as well as C 1s and O 1s peaks from CNTs (Fig. 1D). This indicates that a layer of Pt nanothorn shell is coated on the CNTs. In addition, the typical Pt 4f peaks consisting of double peaks can be split into four peaks. The peaks located at 71.7 eV and 74.5 eV are assigned to Pt $4f_{(7/2)}$ and Pt $4f_{(5/2)}$ in the metallic state, while the peaks at 71.2 eV and 75.5 eV represent Pt $4f_{(7/2)}$ and Pt $4f_{(5/2)}$ corresponding to Pt^{2+} (Fig. 1E).[32,33] The atomic ratio of Pt/Pt^{2+} is about 3.1, indicating the predominant metallic Pt species in the nanowires. The crystalline lattices of the PtNTs were analyzed by X-ray diffraction (Fig. 1F). There are four diffraction peaks located at 39.6°, 45.9°, 68.1°, and 81.5°, attributed to the (1,1,1), (1,0,0), (1,1,0) and (3,1,1) planes of the face-centered cubic (fcc) Pt,[34] respectively. Meanwhile, the diffraction peak at the (1,1,0) lattice is much stronger than the other peaks, implying that the PtNTs had highly active catalytic activity.[35]

To achieve highly active PtNTs, the interfacial reaction conditions were optimized mainly by tuning the interfacial reaction time (Fig. 2). With an increase in the reaction time, nanothorns are produced gradually and are absorbed tightly on the CNTs. After 3 h of reaction, a layer of short Pt nanothorns coats the surface of the CNTs completely (Fig. 2A). Further growth leading to the increasing length of the nanothorns and optimal PtNTs is achieved after 6 h (Fig. 1B). The length–diameter ratio of the PtNTs prepared with 6 h of reaction process is clearly larger than for the other samples. If the reaction time is prolonged again, lots of Pt atoms are deposited on the CNTs and gradually form an irregular aggregation. The nanostructures prepared by 12 h of reaction exhibit a rough surface with nanoscale particles below 100 nm, while the sizes of the surface particles increase to over 300 nm after 24 h of reaction (Fig. 2B and C). Further growth leads to larger particle aggregates without an obvious regular morphology (Fig. 2D). On the other hand, the growing nanoparticles in the bulk solution were also characterized by TEM (Fig. S2, ESI†). It was found that there are large amounts only of tiny Pt nanoparticles in the solution. The formation of unique PtNTs has a close relationship with the interfacial reaction process. In the present work, the CNTs/PtNTs hybrid prepared by 6 h of reaction was selected as the optimal sample to study their electrocatalytic properties for methanol oxidation.

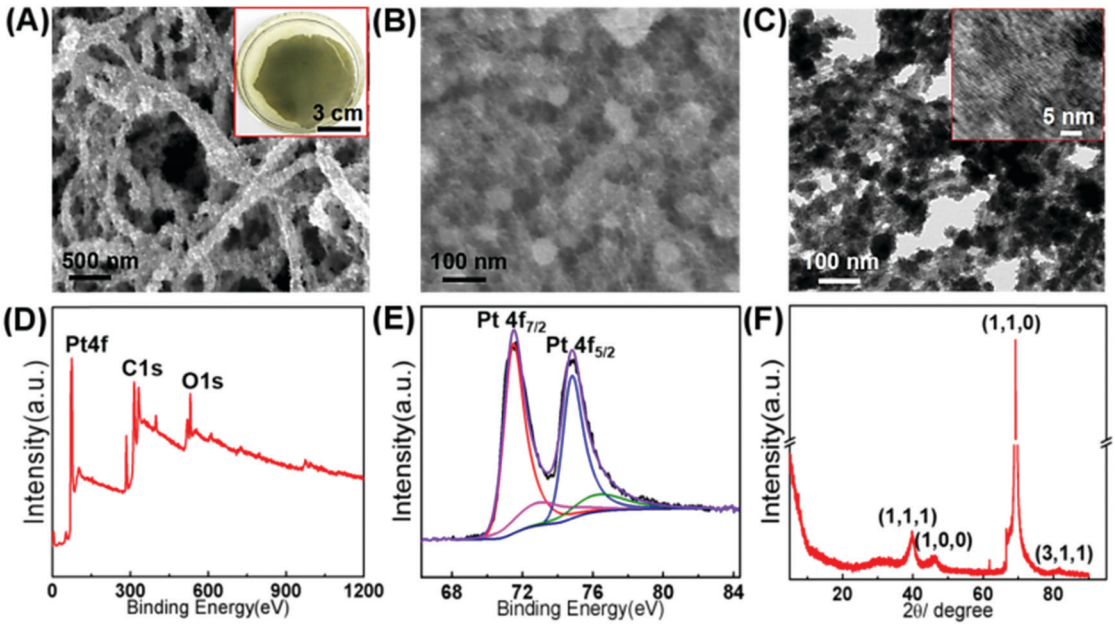

Fig. 1 (A) SEM images of the CNTs/PtNTs film prepared by a 6 h reaction and its high-resolution image (B). The inset in A is a picture of the CNTs/PtNTs composite film floating on water. (C) TEM image of the CNTs/PtNTs composite film. (D and E) XPS spectrum of the CNTs/PtNTs composite film and Pt 4f spectrum. (F) XRD pattern of PtNTs on the CNTs.

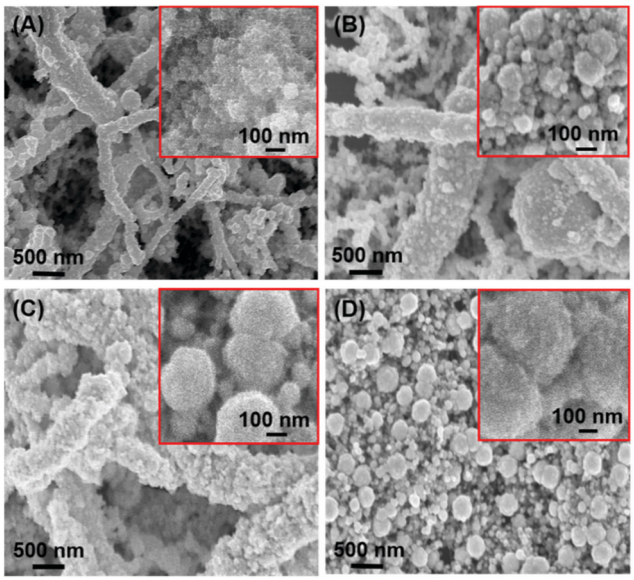

Fig. 2 SEM images of the CNTs/PtNTs hybrid prepared with different reaction times: (A) 3 h, (B) 12 h, (C) 24 h and (D) 36 h.

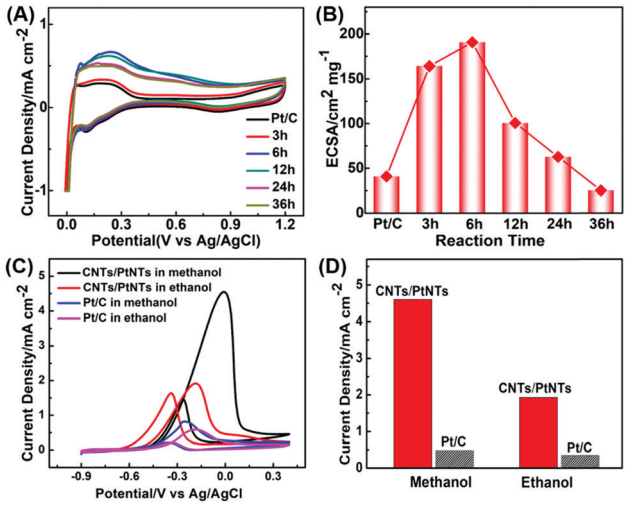

Fig. 3 (A) CV curves of a CNTs/PtNTs modified electrode in 0.5 M H_2SO_4. (B) The ECSA values of the CNTs/PtNTs hybrid prepared with different reaction times. (C) CV curves of CNTs/PtNTs/GCE and commercial Pt/C in 0.5 M NaOH solution containing 2 M alcohol. (D) The maximum current density values of CNTs/PtNTs/GCE and Pt/C in methanol and ethanol.

The electrochemically active surface area (ECSA) of the CNTs/PtNTs was determined by cyclic voltammetry (CV) measurement based on an adsorption/stripping process in 0.5 M H_2SO_4 solution (Fig. 3A). The ECSA value is calculated according to the following eqn (1).[36]

$$\mathrm{ECSA} = (S_H/V)/[C \cdot M_{Pt}] \quad (1)$$

where S_H is the charge for the hydrogen adsorption region, M_{Pt} is the weight of Pt (mg) on the working electrode, V is the scan rate (50 mV s^{-1}), and C is the charge density of Pt and represents the charge that is required to oxidize a monolayer of H_2 on a bright Pt surface. Based on the previous report, the value of C is 0.21 mC cm^{-2} for Pt nanoparticles.[37] The charge of hydrogen adsorption was obtained by calculating the area from 0 to 0.3 V, while the weight of Pt was obtained by the ICP-MS method (Table S1, ESI†). The maximum ECSA value of CNTs/PtNTs is about 190.5 cm^2 mg^{-1}, corresponding to the PtNTs prepared by a 6 h interfacial reaction (Fig. 1B). In addition, the short PtNTs prepared by 3 h of reaction also have a relatively high ECSA value of 164.01 cm^2 mg^{-1} (Table S1, ESI†). By contrast, other irregular Pt nanostructures show a lower ECSA value. This indicates that nanothorn structures with a high specific surface area exhibit a high ECSA value.

The CNTs/PtNTs with a high specific surface area and active lattice planes are expected to be efficient electrocatalysts. To investigate the catalytic effects of CNTs/PtNTs, a typical electrocatalytic methanol and ethanol oxidation in alkaline solution serves as a model. In the electrocatalytic methanol oxidation by CNTs/PtNTs, as illustrated in Fig. 3C, an anodic peak that is typically assigned to the oxidation of methanol appears at around 0 V in the forward scan. In addition, a smaller peak in the reverse scan at around −0.19 V arises from further oxidation of the intermediate products. Under the same alcohol concentration in NaOH solution, the electrocatalytic ability of CNTs/PtNTs on both methanol and ethanol oxidation is higher than that of a commercial Pt/C catalyst (Fig. 3D). Compared with the case of ethanol oxidation, the methanol oxidation current density is much higher, which indicates the higher catalytic ability of PtNTs for methanol oxidation.

During the electrocatalytic methanol oxidation, the current density increases gradually with an increase in the concentration of methanol. As shown in Fig. 4A and B, the current density is enhanced nonlinearly with an increase in methanol concentration and approaches a maximum value of 4.5 mA cm^{-2} in 2 M methanol. Although the oxidation current density increases obviously, the onset potential for methanol electro-oxidation shifts positively to a small degree. To further investigate the practicality of CNTs/PtNTs film, the stability was evaluated by a recycled CV process and long-term electrocatalysis. Fig. 4C shows 100 cycles of CV measurement in a potential range from −0.9 to 0.4 V at 50 mV s^{-1}. The anodic current at 0 V during the forward scan was extracted and plotted against the cycle number, as depicted in the inset in Fig. 4C. After 100 cycles of CV measurements, the CV curves show negligible changes and the maximum oxidation current density remains almost constant at 4.5 mA cm^{-2}, suggesting the good stability and reproducibility of CNTs/PtNTs. The anti-poisoning abilities of CNTs/PtNTs for methanol oxidation were evaluated by chronoamperometric measurements at a potential of 0.05 V for 1000 s. The electrocatalytic oxidation reaction was performed in a mixed solution containing 2 M of methanol and 0.5 M of NaOH (Fig. 4D). Initially, the current on both CNTs/PtNTs and Pt/C catalysts decays rapidly, probably arising from the cumulative adsorption of poisonous carbonaceous intermediates on the surface of the catalyst.[38] Compared with Pt/C catalysis, CNTs/PtNTs exhibit a higher current density and slower decay rate over the whole scanning range. This indicates that CNTs/PtNTs have higher catalytic activity and better stability for electrocatalytic methanol oxidation than a commercial Pt/C catalyst.[39]

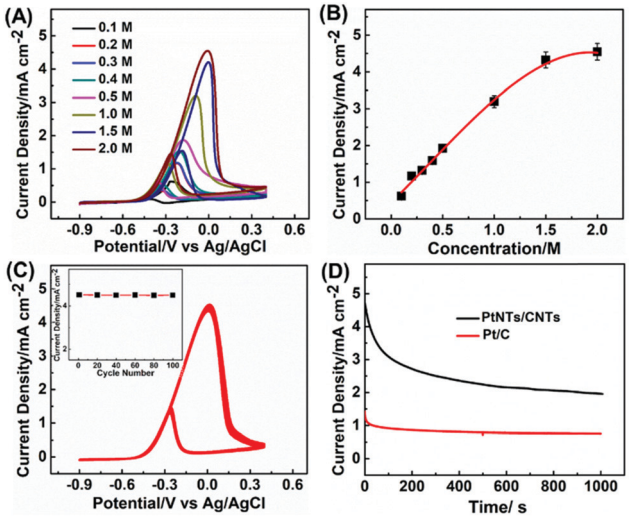

Fig. 4 (A) CV curves of CNTs/PtNTs/GCE in 0.5 M NaOH containing different methanol content. (B) A plot of oxide current density against the concentration of methanol. (C) 100 cycles of CV measurements of CNTs/PtNTs/GCE. The inset in (C) represents the anodic current density at 0.05 V. (D) Chronoamperometric measurements of CNTs/PtNTs and Pt/C.

Apart from methanol, ethanol is another general resource candidate for an alcohol fuel cell. The electrocatalytic effects of PtNTs on ethanol oxidation was also studied in alkaline media (Fig. 5).[40] In the CV measurement, the ethanol oxidation current density increases gradually with an increase in ethanol concentration and reaches a maximum value of 1.9 mA cm^{-2} at a low concentration of 0.5 M (Fig. 5A and B). The current density is lower than that in the case of methanol oxidation. After 100 cycles of CV measurements, the current density on CNTs/PtNTs/GCE shows a distinct variation (Fig. 5C), exhibiting unstable electrocatalytic activity. In the chronoamperometric test results, the decay rate of

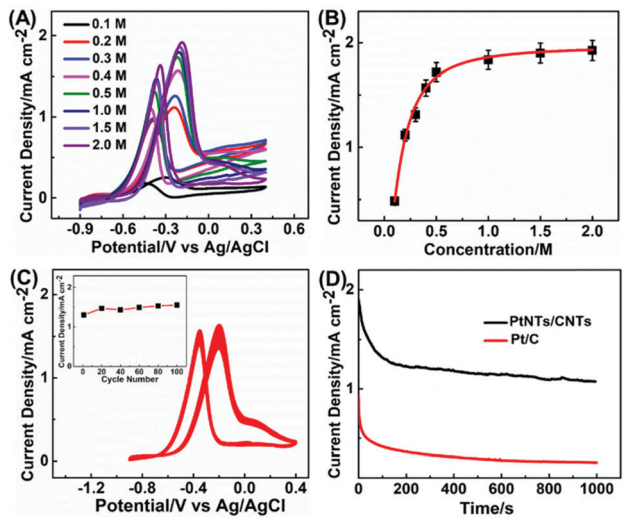

Fig. 5 (A) CV curves of CNTs/PtNTs/GCE with different ethanol content. (B) A plot of oxide peak current density against the concentration of ethanol. (C) 100 cycles of CV measurements of CNTs/PtNTs/GCE. The inset in (C) represents the anodic current density at −0.18 V. (D) Chronoamperometric measurements of CNTs/PtNTs and Pt/C.

CNTs/PtNTs in the ethanol oxidation is similar to Pt/C, although CNTs/PtNTs generate a higher catalytic current density (Fig. 5D). Compared with the case of methanol oxidation, the electrocatalytic ability and stability of CNTs/PtNTs for ethanol oxidation is much lower. The achieved CNTs/PtNTs are more suitable for electrocatalytic methanol oxidation.

4. Conclusions

In summary, a unique and facile air/water interfacial reaction strategy is demonstrated for effectively synthesizing Pt nanowires, which are *in situ* loaded onto a macroscopic flexible CNT film in high density. The resultant freestanding CNTs/PtNTs composite film can be transferred stably onto an electrode surface. The CNTs/PtNTs composite film with a high ECSA value of 190.5 cm^2 mg^{-1} exhibits high electrocatalytic ability for alcohol oxidation. The current density of catalytic methanol oxidation is as high as 4.5 mA cm^{-2} in 2 M methanol. Meanwhile, the prepared CNTs/PtNTs composite film displays good catalytic stability and durability. This work provides a cost-effective and convenient method to achieve a Pt nanowire electrocatalyst candidate for methanol fuel cells, showing good potential for the robust fabrication of a composite film catalyst for methanol fuel cells.

Conflicts of interest

There are no conflicts to declare.

Acknowledgements

The authors thank the Natural Science Foundation of China (Grant No. 51603219, 51473179, 11604346), the Ningbo Science and Technology Bureau (Grant No. 2017D10001, 2015C110031), the Bureau of Frontier Science and Education of the Chinese Academy of Sciences (Grant No. QYZDB-SSW-SLH036), and the Youth Innovation Promotion Association of the Chinese Academy of Sciences (Grant No. 2016268, 2017337) for financial support.

References

1 H. Huang and X. Wang, *J. Mater. Chem. A*, 2014, **2**, 6266–6291.
2 S. Yan, S. Zhang, W. Zhang, J. Li, L. Gao, Y. Yang and Y. Gao, *J. Phys. Chem. C*, 2014, **118**, 29845–29853.
3 L. Lin, Q. Zhu and A. W. Xu, *J. Am. Chem. Soc.*, 2014, **136**, 11027–11033.
4 R. Jasinski, *Nature*, 1964, **201**, 1212.
5 V. R. Stamenkovic, B. Fowler, B. S. Mun, G. Wang, P. N. Ross, C. A. Lucas and N. M. Markovic, *Science*, 2007, **315**, 493–497.
6 S. J. Guo, D. G. Li, H. Y. Zhu, S. Zhang, N. M. Markovic, V. R. Stamenkovic and S. H. Sun, *Angew. Chem., Int. Ed.*, 2013, **52**, 3465–3468.
7 K. A. Kuttiyiel, K. Sasaki, Y. M. Choi, D. Su, P. Liu and R. R. Adzic, *Nano Lett.*, 2012, **12**, 6266–6271.

8 X. Li, H. J. Wang, H. Yu, Z. W. Liu and F. Peng, *J. Power Sources*, 2014, **260**, 1–5.
9 R. Ojani, E. Hasheminejad and J. B. Raoof, *Energy*, 2015, **90**, 1122–1131.
10 Y. J. Song, S. B. Han and K. W. Park, *Mater. Lett.*, 2010, **64**, 1981–1984.
11 M. A. Hoque, F. M. Hassan, A. M. Jauhar, G. P. Jiang, M. Pritzker, J. Y. Choi, S. Knights, S. Y. Ye and Z. W. Chen, *ACS Sustainable Chem. Eng.*, 2018, **6**, 93–98.
12 C. W. Zhang, J. F. Chen and L. B. Xu, *Mater. Lett.*, 2018, **223**, 97–101.
13 M. N. Ding, Y. Liu, G. M. Wang, Z. P. Zhao, A. X. Yin, Q. Y. He, Y. Huang and X. F. Duan, *Small*, 2017, **13**, 1602969.
14 M. Olek, J. Ostrander, S. Jurga, H. Mohwaid, N. Kotov, K. Kempa and M. Giersig, *Nano Lett.*, 2004, **4**, 1889–1895.
15 W. J. Ma, L. Song, R. Yang, T. H. Zhang, Y. C. Zhao, L. F. Sun, Y. Ran, D. F. Liu, L. F. Liu, J. Shen, Z. X. Zhang, Y. J. Xiang, W. Y. Zhou and S. S. Xie, *Nano Lett.*, 2007, **7**, 2307–2311.
16 Z. Shi, X. J. Chen, X. W. Wang, T. Zhang and J. Jin, *Adv. Funct. Mater.*, 2011, **21**, 4358–4363.
17 X. M. Li, T. T. Yang, Y. Yang, J. Zhu, L. Li, F. E. Alam, X. Li, K. L. Wang, H. Y. Cheng, C. T. Lin, Y. Fang and H. W. Zhu, *Adv. Funct. Mater.*, 2016, **26**, 1322–1329.
18 P. Xiao, J. C. Gu, C. J. Wan, S. Wang, J. He, J. W. Zhang, Y. J. Huang, S. W. Kuo and T. Chen, *Chem. Mater.*, 2016, **28**, 7125–7133.
19 F. L. Qu, M. H. Yang, G. L. Shen and R. Q. Yu, *Biosens. Bioelectron.*, 2007, **22**, 1749–1755.
20 Y. H. Liu, D. L. Tang, K. H. Cao, L. Yu, J. Han and Q. Xu, *J. Catal.*, 2018, **360**, 250–260.
21 C. J. Jin, J. Han, F. Y. Chu, X. Wang and R. Guo, *Langmuir*, 2017, **33**, 4520–4527.
22 Z. K. Zheng, T. C. Nottbohm, T. Andrey, H. K. Muzik, A. Beyer, M. Heilemann, M. Sauer and A. Golzhauser, *Angew. Chem., Int. Ed.*, 2010, **49**, 8493–8497.
23 Y. Li, X. Z. Ye, Y. R. Ma and L. M. Qi, *Small*, 2015, **11**, 1183–1188.
24 L. Zhang, Y. Z. Tao, P. Xiao, L. W. Dai, L. P. Song, Y. J. Huang, J. W. Zhang, S. W. Kuo and T. Chen, *Adv. Mater. Interfaces*, 2017, **4**, 1601105.
25 S. H. Sun, G. X. Zhang, Y. Zhong, H. Liu, R. Y. Li, X. R. Zhou and X. L. Sun, *Chem. Commun.*, 2009, 7048–7050.
26 X. Wang, W. Wang, Z. Qi, C. Zhao, H. Ji and Z. Zhang, *Electrochem. Commun.*, 2009, **11**, 1896–1899.
27 Y. Nie, L. Li and Z. Wei, *Chem. Soc. Rev.*, 2015, **44**, 2168–2201.
28 H. Vedala, D. C. Sorescu, G. P. Kotchey and A. Star, *Nano Lett.*, 2011, **11**, 2342–2347.
29 S. H. Xu, Z. S. Li, F. L. Lei, Y. L. Wang, Y. X. Xie and S. Lin, *Appl. Surf. Sci.*, 2017, **426**, 351–359.
30 L. Zhang, P. Xiao, W. Lu, J. W. Zhang, J. C. Gu, Y. J. Huang and T. Chen, *Adv. Mater. Interfaces*, 2016, **3**, 1600170.
31 Y. Xin, J. G. Liu, Y. Zhou, W. Liu, J. Gao, Y. Xie, Y. Yin and Z. Zou, *J. Power Sources*, 2011, **196**, 1012–1018.
32 Q. An, J. Qian, R. R. Nielsen, L. Sementa, G. Barcato, F. R. Negreiros, A. Fortunelli and W. A. Goddard, *J. Mater. Chem. A*, 2016, **4**, 12036–12045.
33 A. Ostroverkh, V. Johánek, P. Kúš, R. Šedivá and V. Matolín, *Langmuir*, 2016, **32**, 6297–6309.
34 S. Manivannan, I. Kang and K. Kim, *Langmuir*, 2016, **32**, 1890–1898.
35 H. Huang, H. Chen, D. Sun and X. Wang, *J. Power Sources*, 2012, **204**, 46–52.
36 C. Bianchini and P. K. Shen, *Chem. Rev.*, 2009, **109**, 4183–4206.
37 L. Zhou, Y. Wang, J. Tang, J. Li, S. Wang, Y. Wang and D. Su, *Microporous Mesoporous Mater.*, 2017, **247**, 116–123.
38 Z. Xu, H. M. Zhang, H. X. Zhong, Q. H. Lu, Y. F. Wang and D. S. Su, *Appl. Catal., B*, 2012, **111**, 264–270.
39 A. Bharti, G. Cheruvally and S. Muliankeezhu, *Int. J. Hydrogen Energy*, 2017, **42**, 11622–11631.
40 S. Yoon, K. Oh, F. D. Liu, J. H. Seo, G. A. Somorjai, J. H. Lee and K. An, *ACS Catal.*, 2018, **8**, 5391–5398.

